# Balancing fluorescence and singlet oxygen formation in push-pull type near-infrared BODIPY photosensitizers

Deckers, Jasper; Cardeynaels, Tom; Doria, Sandra; Tumanov, Nikolay; Lapini, Andrea; Ethirajan, Anitha; Ameloot, Marcel; Wouters, Johan; Di Donato, Mariangela; Champagne, Benoît; Maes, Wouter

*Published in:*
Journal of Materials Chemistry C

*DOI:*
10.1039/d2tc01526a

*Publication date:*
2022

*Document Version*
Publisher's PDF, also known as Version of record

Journal of Materials Chemistry C

ROYAL SOCIETY OF CHEMISTRY

PAPER

View Article Online
View Journal | View Issue



Cite this: J. Mater. Chem. C, 2022, 10, 9344

# Balancing fluorescence and singlet oxygen formation in push–pull type near-infrared BODIPY photosensitizers†

Jasper Deckers, ‡[abc] Tom Cardeynaels, ‡[abcd] Sandra Doria,[ef] Nikolay Tumanov,[g] Andrea Lapini,[eh] Anitha Ethirajan,[bi] Marcel Ameloot,[j] Johan Wouters,[g] Mariangela Di Donato,[ef] Benoît Champagne[d] and Wouter Maes *[abc]

Received 13th April 2022,
Accepted 6th June 2022

DOI: 10.1039/d2tc01526a

rsc.li/materials-c

Boron dipyrromethene dyes are highly attractive for image-guided photodynamic therapy. Nevertheless, their clinical breakthrough as theranostic agents is still obstructed by several limitations. Here, we report a series of strongly absorbing, heavy-atom-free, distyryl-BODIPY donor–acceptor dyads operating within the phototherapeutic window. Whereas diphenylamine and carbazole donors lead to strong fluorescence, dimethylacridine, phenoxazine, and phenothiazine units afford a decent fluorescence combined with the efficient formation of singlet oxygen. Dedicated photophysical analysis and quantum-chemical calculations are performed to elucidate the excited state dynamics responsible for the pronounced differences within the BODIPY series. Femtosecond transient absorption spectra reveal the nature of the excited state processes and the involvement of charge-transfer states in triplet formation.



## Introduction

Singlet oxygen (denoted as $O_2(^1\Delta_g)$, shortened as $^1O_2$) is a powerful reagent that is employed in the manufacture of fine chemicals, wastewater treatment, blood sterilization, and the production of specific insecticides and herbicides, among others.[1] Furthermore, the combination of its high reactivity, related short lifetime, and slow diffusion rate in biological media, renders $^1O_2$ the protagonist in photodynamic therapy (PDT).[2,3] In PDT, light is used to activate a photosensitizer (PS), which then produces reactive oxygen species (ROS) through different mechanisms.[4] These ROS result in the selective destruction of tumor cells at the irradiation site, allowing PDT to be used for cancer therapy. Furthermore, PDT can also be employed in a broader sense for treating ophthalmic and dermatologic diseases, bacterial and fungal infections, and the inactivation of viruses.[5–12] Whereas type I PDT investigates ROS formation upon direct interaction of the activated PS with a substrate, most studies focus on the type II PDT process since $^1O_2$ is considered the leading cytotoxic agent.[13] In more detail, the PS is excited with photons of a suitable wavelength, thereby achieving an electronically excited singlet state ($S_n$). For $^1O_2$ formation, intersystem crossing (ISC) is required to obtain a triplet state ($T_n$) from which, after fast internal conversion to the first triplet state ($T_1$), energy transfer to molecular oxygen ($O_2(^3\Sigma_g^-)$ or $^3O_2$) can occur.[14] As ISC is a spin-forbidden transition, the quest for compounds with efficient triplet formation remains a crucial research topic.

[a] UHasselt – Hasselt University, Institute for Materials Research (IMO), Design & Synthesis of Organic Semiconductors (DSOS), Agoralaan, 3590 Diepenbeek, Belgium. E-mail: wouter.maes@uhasselt.be
[b] IMEC, Associated Lab IMOMEC, Wetenschapspark 1, 3590 Diepenbeek, Belgium
[c] Energyville, Thorpark, 3600 Genk, Belgium
[d] UNamur – University of Namur, Namur Institute of Structured Matter, Theoretical and Structural Physical Chemistry Unit, Laboratory of Theoretical Chemistry (LTC), Rue de Bruxelles 61, 5000 Namur, Belgium
[e] European Laboratory for Non-Linear Spectroscopy (LENS), Via Nello Carrara 1, 50019 Sesto Fiorentino (FI), Italy
[f] Instituto di Chimica dei Composti OrganoMetallici (ICCOM-CNR), Via Madonna Del Piano 10, 50019 Sesto Fiorentino (FI), Italy
[g] UNamur – University of Namur, Namur Medicine and Drug Innovation Center (NAMEDIC), Namur Research Institute for Life Sciences (NARILIS), Namur Institute of Structured Matter (NISM), Rue de Bruxelles 61, 5000 Namur, Belgium
[h] Department of Chemistry, Life Science and Environmental Sustainability, University of Parma, Parco Area delle Scienze, 17/A, 43124 Parma, Italy
[i] UHasselt – Hasselt University, Institute for Materials Research (IMO), Nano-Biophysics and Soft Matter Interfaces (NSI), Wetenschapspark 1, 3590 Diepenbeek, Belgium
[j] UHasselt – Hasselt University, Biomedical Research Institute (BIOMED), Agoralaan, 3590 Diepenbeek, Belgium

† Electronic supplementary information (ESI) available: Materials and methods, detailed BODIPY dyad synthesis procedures and characterization data, additional (TD)DFT data and figures, single-crystal X-ray structures, singlet oxygen generation plots, additional absorption and emission spectra and data, additional transient absorption spectra and data, and $^1H/^{13}C$ NMR spectra. CCDC 2122792–2122794. For ESI and crystallographic data in CIF or other electronic format see DOI: https://doi.org/10.1039/d2tc01526a

‡ These authors contributed equally.

Throughout the years, a vast amount of organic photosensitizers have been reported.[15–23] Among these promising molecules, 4,4-difluoro-4-bora-3*a*,4*a*-diaza-*s*-indacenes (commonly indicated as boron dipyrromethenes or BODIPYs) are one of the most prominent examples.[24–36] Their high molar extinction coefficients, (photo)chemical stability, and easily tunable photophysical properties make them attractive PSs.[37–39] However, typically high fluorescence quantum yields ($\Phi_f$) of BODIPY dyes imply ISC restrictions as these are competing decay processes for the first singlet excited state. The most encountered solution is the introduction of bromine, iodine, or transition metal complexes on the BODIPY structure, thereby increasing spin–orbit coupling (SOC) through the so-called heavy-atom effect.[40–43] Nevertheless, related additional synthetic efforts and costs, shortened triplet state lifetimes, low photostability, and increased dark cytotoxicity provided an impetus to search for alternative ISC mechanisms.[44–46] In this way, novel BODIPY PSs were developed, based on reduced singlet–triplet energy gaps ($\Delta E_{ST}$), spin converters, radical-enhanced ISC, radical pair ISC, twisted π-conjugation-induced ISC, and spin–orbit charge-transfer ISC (SOCT-ISC).[40–42,47,48] These alternative approaches open the possibility for theranostic applications as subtle engineering of the energy levels can allow triplet population and singlet emission to coexist. In PDT, these self-reporting PSs present an appealing step toward personalized cancer treatment, enabling the combination of diagnosis and therapy to localize the target, monitor the therapeutic progression, and improve drug dosimetry.[49–51]

Another essential feature for PDT PSs is their activity in the near-infrared (NIR) spectral region. Shorter wavelengths are more prone to scattering and several tissue chromophores will filter the UV-VIS part of the incoming light.[14,52,53] Wavelengths between 600 and 800 nm are desired to limit light scattering, reduce background signals, and enhance tissue penetration depths.[54] Although strategies to bathochromically shift the absorption and emission properties are well-known for BODIPY dyes, it is not straightforward to combine strong $^1O_2$ production with a decent brightness in the phototherapeutic region.[55–58] Hence, only a handful of NIR-photoactive heavy-atom-free dual-functioning BODIPY PSs have been developed so far.[59–66]

Recently, we reported a series of distyryl–BODIPY–acridine dyads, active in the phototherapeutic window, showing balanced brightness and phototoxic power.[66] Concentration-dependent fluorescence experiments suggested the involvement of 'exciplex'[67] energy states in the decay mechanism. Relatively long exciplex state lifetimes, combined with their polar nature, would render them a suitable intermediate in the ISC process, as previously reported for other donor–acceptor BODIPY systems.[68–70] To gain more insights into the relationship between the molecular structure and the photophysical properties of distyryl–BODIPY dyads, we report here on the development of a new series of donor–acceptor type BODIPY dyads wherein the electron donor moieties are varied. Diphenylamine and carbazole donors were found to afford high fluorescence quantum yields ($\Phi_f \sim$ 45–75%) in polar and apolar solutions. However, negligible $^1O_2$ formation was observed for these systems. In line with our previous results for dimethylacridine, incorporation of phenoxazine and phenothiazine donors resulted in efficient PSs, with $^1O_2$ quantum yields ($\Phi_\Delta$) ranging from 33 to 47% in both chloroform and toluene solution. Fluorescence emission was quenched in chloroform for these dyads, but this feature was retained in toluene, resulting in $\Phi_f$ values around 50%. Hence, these distyryl-BODIPY dyads are interesting self-reporting PDT PSs. Femtosecond transient absorption spectroscopy (fs-TAS) was used to gain detailed insights in the excited state processes, suggesting the involvement of charge-transfer (CT) states in the ultrafast dynamics.

## Results and discussion

### Photosensitizer design and synthesis

The molecular design of the newly developed systems was inspired on the recently reported distyryl–BODIPY–acridine donor–acceptor (D–A) dyad **5a**, possessing both an attractive brightness and phototoxicity within the phototherapeutic window.[66] The donor end group (dimethylacridine **3a**) was deemed essential to realize exciplex formation and to allow for efficient ISC to occur. To further elucidate the origin of the ISC and the influence of the molecular design on this process, a variety of alternative donor units were now screened, going from phenoxazine (**3b**) to phenothiazine (**3c**), diphenylamine (**3d**), carbazole (**3e**), and 3,6-di-*tert*-butylcarbazole (**3f**) (Scheme 1).

For the material synthesis, donor moieties **3a–f** were first combined with 4-bromobenzaldehyde in a Buchwald–Hartwig amination reaction using tris(dibenzylideneacetone)dipalladium(0) ($Pd_2(dba)_3$) and 1,1′-bis(diphenylphosphino)ferrocene (dppf) as the catalytic system to yield aldehydes **4a–f** in moderate to high yields (59–92%). The highly fluorescent 1,3,5,7-tetramethyl-BODIPY core **2** was obtained from 2,4-dimethylpyrrole (**1**) according to a literature procedure.[71] This *meso*-mesityl-BODIPY structure was chosen for its facile synthesis and good solubility of the resulting BODIPY dyads. The relatively acidic protons of the α-methyl groups enable a Knoevenagel-type condensation to afford the desired distyryl-BODIPY dyads **5a–f**. A short and easy synthetic procedure, comprising five-minute microwave irradiation in the presence of glacial acetic acid and piperidine, resulted in good to high yields (54–91%). The reaction conditions were optimized previously for dimethylacridine **3a**.[66] For a detailed description of the synthesis protocols and material characterization data, we refer to the ESI.†

### Structural analysis

Density functional theory (DFT) calculations were performed to analyze the molecular structures of the BODIPY dyads with varying donor units. All geometries were optimized using the M06-2X exchange–correlation functional with the 6-311G(d) basis set and the polarizable continuum model (PCM) to simulate the moderately polar environment of a chloroform solution. Vibrational analysis was performed to confirm that all geometries correspond to minima on the potential energy surfaces. By varying the attached donor end groups in the

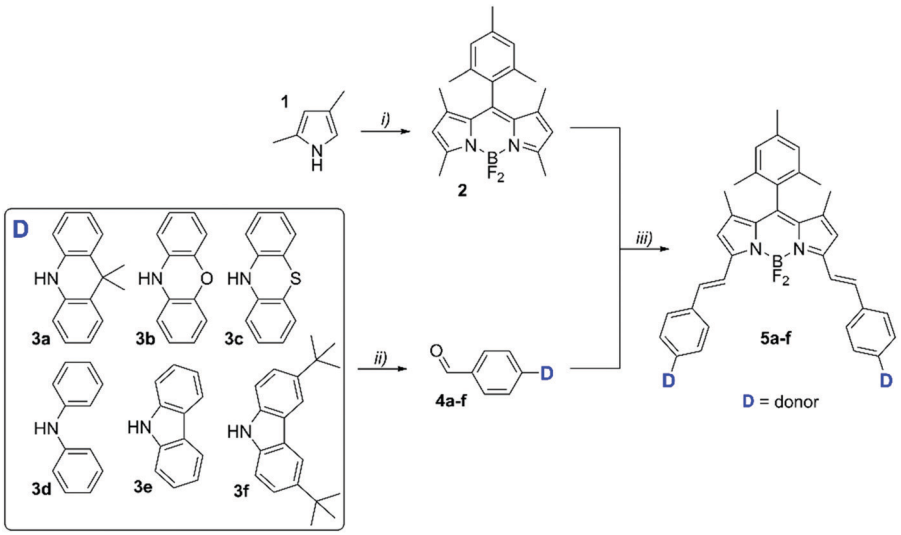


Scheme 1 Synthesis of BODIPY dyads **5a–f** and their respective building blocks: (i) 2,4,6-trimethylbenzaldehyde, trifluoroacetic acid, dry $CH_2Cl_2$, inert atm, 3 h at 0 °C; 2,3-dichloro-5,6-dicyano-1,4-benzoquinone (DDQ), 20 min at 0 °C, 1 h at room temperature (RT); $Et_3N$, $BF_3{\cdot}OEt_2$, 12 h at RT (72%); (ii) 4-bromobenzaldehyde, $Pd_2(dba)_3$, $Cs_2CO_3$, dppf, dry toluene, inert atm, 16 h at 100 °C (59–92%); (iii) glacial acetic acid, piperidine, dry *N*,*N*-dimethylformamide (DMF), inert atm, 5 min at 150 °C (microwave irradiation) (54–91%).

distyryl–BODIPY dyads, large differences in the dihedral angles between the donor and acceptor moieties were observed, ranging from 34° for the diphenylamine unit (**5d**) to 90° for dimethylacridine, phenoxazine, and phenothiazine (**5a–c**) (Fig. 1). This torsion angle is the same for both arms. All donor units are planar, with the exception of phenothiazine (**5c**), which is bent with an angle of 33°, and diphenylamine (**5d**), which has an angle of 70° between the two phenyl rings. The frontier molecular orbitals (Fig. S1 and S2, ESI†) show that the highest occupied molecular orbital (HOMO) and the lowest unoccupied molecular orbital (LUMO) are located on the distyryl-BODIPY unit for **5a–f**, except for the HOMO orbital of **5b**, which is located on one of the phenoxazine units. The HOMO−1 and HOMO−2 orbitals are mainly localized on the respective donor units, again except for BODIPY **5b**, for which the HOMO−2 orbitals are located on the distyryl-BODIPY core. This discrepancy for **5b** can be explained by considering the energy levels of the various orbitals (Table S1, ESI†). The quasi-degenerate HOMO−2, HOMO−1, and HOMO energies are within 0.05 eV from each other, allowing an inversion between the character of HOMO/HOMO−1 (both localized on the donor unit) and HOMO−2 (localized on the styryl-BODIPY moiety).[72] The smaller dihedral angles in BODIPYs **5d–f** lead to increased HOMO delocalization toward the donor unit (Fig. S2, ESI†). In all compounds, the mesityl *meso*-group is nearly perpendicular to the rest of the BODIPY core, electronically decoupled from it.

Single crystals were obtained for BODIPYs **5a**, **5c**, and **5e** (Fig. S3–S5 and Table S2, ESI†). The single-crystal X-ray structures confirm the molecular structures of the designed BODIPY units and also indicate that the correct geometrical conformations are probed for the time-dependent DFT (TDDFT) calculations (*vide infra*). In addition, the dihedral angles between the donor and acceptor groups were found to be 89° for **5a**, 80° for

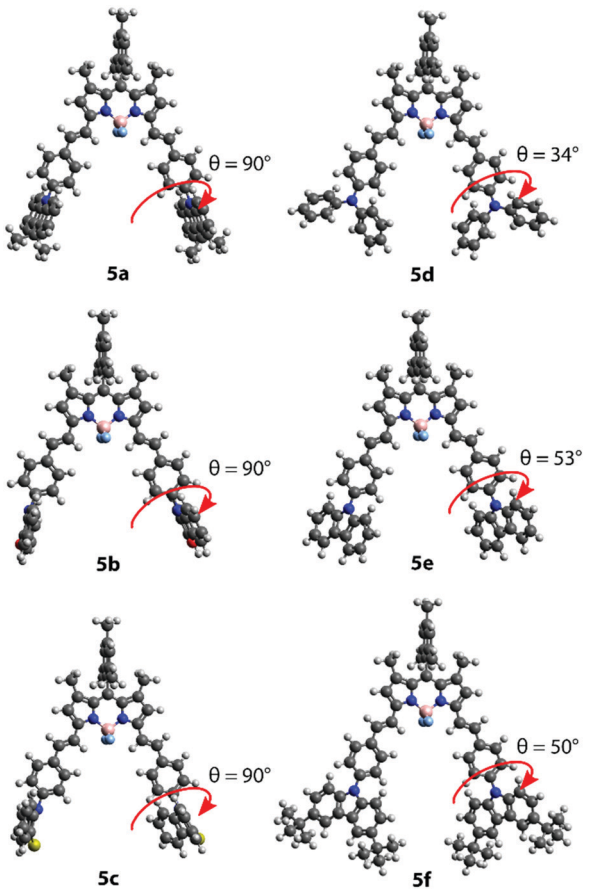


Fig. 1 Optimized ground-state geometries for BODIPYs **5a–f** with the dihedral angles between the donor units and the distyryl-BODIPY core indicated by red arrows.

 

**5c**, and 70° for **5e**, which is in good agreement with the DFT calculations (Fig. 1). In contrast to the findings of the DFT geometry optimization, the dimethylacridine unit is slightly bent (14°) in the single crystal structure. The bending of phenothiazine is 21° in the crystal structure, which is slightly less than observed in the geometry optimization.

### TDDFT calculations

To assess the optical properties of BODIPY dyads **5a–f**, TDDFT calculations were performed using M06-2X as the exchange-correlation functional and 6-311G(d) as the basis set. The PCM was applied to simulate the solution measurement conditions in chloroform. The lowest singlet vertical excitation energies for **5a–f** are all in the region of 2.01–2.16 eV (617–573 nm) (Table 1). The second singlet vertical excitation energies are considerably larger ($\Delta E_{S1-S2}$ = 0.85–1.20 eV), making it unlikely that the $S_2$ states play a significant role in the photophysical properties. The two lowest triplet vertical excitation energies vary from 1.15–1.20 eV and 2.30–2.56 eV, respectively. This means that the first singlet vertical excitation energy is in between the two first triplet vertical excitation energies in all cases, as previously observed for the dimethylacridine-containing dyad **5a**.[66] BODIPY dyads **5d–f** show slightly lower first singlet and first triplet vertical excitation energies with respect to BODIPYs **5a–c**. This is likely due to the smaller dihedral angles for these donor units, resulting in delocalization of the HOMO from the BODIPY part onto the donor unit, which is not seen for BODIPYs **5a–c** (Fig. S1 and S2, ESI†). The increase in HOMO delocalization gives rise to a more extended π-conjugated system for the transition as the first singlet excited state is of HOMO → LUMO character for all dyads, except for **5b** (HOMO−2 → LUMO), for which we already denoted the inversion between the topologies of the HOMO and HOMO−2. The first singlet excited state has a large oscillator strength, which indicates high molar absorptivities (*i.e.* strong absorption).

To probe the CT characteristics of the push–pull BODIPY series, the ground and excited state electron densities were evaluated according to the work of Le Bahers *et al.*, using the distance over which charge is transferred ($d_{CT}$) and the change in dipole moment ($\Delta\mu$) as figures of merit (Table 2).[73] As the name implies, excitations with a higher degree of CT character will have larger values for $d_{CT}$ since the charge is transferred over a certain distance as opposed to localized excitations in which the charge is merely redistributed over a given part of the molecule. Furthermore, CT excitations are characterized by a more significant $\Delta\mu$ as the charge is transferred from one part of the molecule to the other, creating areas with reduced and increased charge density distributions. For dyads **5a–f**, the $S_0 \rightarrow S_2$ transition seems to be the only excitation with CT character, as indicated by the relatively large $d_{CT}$ ($\geq$ 4.22 Å) and $\Delta\mu$ ($\geq$ 18.4 D) values with respect to those for the other transitions ($\leq$ 2.71 Å for $d_{CT}$ and $\leq$ 7.2 D for $\Delta\mu$) (Table 2). As discussed before, the vertical excitation energy for the $S_0 \rightarrow S_2$ transition is much higher than for $S_0 \rightarrow S_1$ (Table 1). Hence, it seems unlikely that the $S_2$ state plays a significant role in the ISC process. These findings can also be visualized by considering the difference between the excited and ground state electron densities, as shown in Fig. S6 and S7 (ESI†).

### Photophysical characterization

The photophysical properties of the six distyryl–BODIPY dyads **5a–f** were investigated in a relatively polar (*i.e.* chloroform) and rather apolar (*i.e.* toluene) medium to explore their absorption and fluorescence behavior and their ability to generate $^1O_2$. Absorption and emission spectra afforded the basic spectral data (Fig. 2 and Table 3). $\Phi_f$ values were obtained at an excitation wavelength of 605 nm, relative to nile blue. $\Phi_\Delta$ data were collected by monitoring the absorbance of 1,3-diphenylisobenzofuran (1,3-DPBF) as a $^1O_2$ scavenger upon excitation at 639 nm (Fig. S8, ESI†). In combination with the molar attenuation coefficients ($\varepsilon$), the brightness (BT) and phototoxic power (PP) were determined. All data reported in Table 3 are mean values from three independent measurements for each compound in the indicated solvent. Only data from the wavelength region of interest are displayed here. For the full absorption spectra, we refer to Fig. S9 and Table S3 (ESI†).

For all BODIPY dyes, absorption maxima in chloroform were found above 630 nm, within the phototherapeutic window.

Table 1 Calculated vertical singlet ($S_1$ and $S_2$) and triplet ($T_1$ and $T_2$) excitation energies and their corresponding oscillator strengths for BODIPYs **5a–f**. The dominant nature of the one-particle excitations is also given

| | $S_0 \rightarrow S_1$ | | | $S_0 \rightarrow S_2$ | | | $S_0 \rightarrow T_1$ | | $S_0 \rightarrow T_2$ | |
|---|---|---|---|---|---|---|---|---|---|---|
| BODIPY | $\Delta E^a$ (eV) | Osc. Str.[b] | Nature[c] | $\Delta E^a$ (eV) | Osc. Str.[b] | Nature[c] | $\Delta E^a$ (eV) | Nature[c] | $\Delta E^a$ (eV) | Nature[c] |
| **5a** | 2.16 (574 nm) | 1.20 | H→L (97%) | 3.08 | 0.00 | H−1→L (85%) | 1.20 | H→L (93%) | 2.55 | H−3→L (50%) |
| **5b** | 2.16 (573 nm) | 1.19 | H−2→L (96%) | 3.01 | 0.00 | H→L (89%) | 1.20 | H−2→L (93%) | 2.56 | H−3→L (49%) |
| **5c** | 2.16 (573 nm) | 1.19 | H→L (97%) | 3.27 | 0.00 | H−1→L (91%) | 1.20 | H→L (94%) | 2.55 | H−5→L (50%) |
| **5d** | 2.01 (617 nm) | 1.27 | H→L (90%) | 2.97 | 1.65 | H−1→L (85%) | 1.15 | H→L (78%) | 2.30 | H−1→L (45%) |
| **5e** | 2.12 (585 nm) | 1.24 | H→L (93%) | 3.32 | 1.53 | H−1→L (77%) | 1.19 | H→L (86%) | 2.49 | H−5→L (32%) |
| **5f** | 2.11 (589 nm) | 1.23 | H→L (89%) | 3.20 | 1.37 | H−1→L (81%) | 1.18 | H→L (80%) | 2.47 | H−5→L (33%) |

[a] Vertical excitation energy (wavelength). [b] Oscillator strength. [c] H = HOMO, L = LUMO.

Table 2 Amount of charge-transfer character ($d_{CT}$) and change in dipole moment ($\Delta\mu$, excited state dipole – ground state dipole) accompanying the $S_0 \rightarrow S_n$ and $S_0 \rightarrow T_n$ ($n$ = 1, 2) transitions in chloroform

| | $S_0 \rightarrow S_1$ | | $S_0 \rightarrow S_2$ | | $S_0 \rightarrow T_1$ | | $S_0 \rightarrow T_2$ | |
|---|---|---|---|---|---|---|---|---|
| BODIPY | $d_{CT}$[a] (Å) | $\Delta\mu$[b] (D) | $d_{CT}$[a] (Å) | $\Delta\mu$[b] (D) | $d_{CT}$[a] (Å) | $\Delta\mu$[b] (D) | $d_{CT}$[a] (Å) | $\Delta\mu$[b] (D) |
| **5a** | 0.64 | 1.3 | 5.14 | 34.7 | 0.64 | 1.7 | 0.38 | 0.6 |
| **5b** | 0.66 | 1.3 | 6.17 | 42.6 | 0.70 | 1.9 | 0.33 | 0.5 |
| **5c** | 0.59 | 1.2 | 6.11 | 41.8 | 0.64 | 1.7 | 0.28 | 0.5 |
| **5d** | 2.09 | 5.3 | 4.22 | 18.4 | 1.02 | 2.9 | 2.71 | 7.2 |
| **5e** | 1.17 | 2.5 | 4.61 | 20.2 | 0.75 | 2.0 | 1.48 | 2.9 |
| **5f** | 1.41 | 3.1 | 4.81 | 23.9 | 0.81 | 2.2 | 1.96 | 4.1 |

[a] Distance over which charge is transferred between the indicated states upon excitation. [b] Change in dipole moment upon excitation.

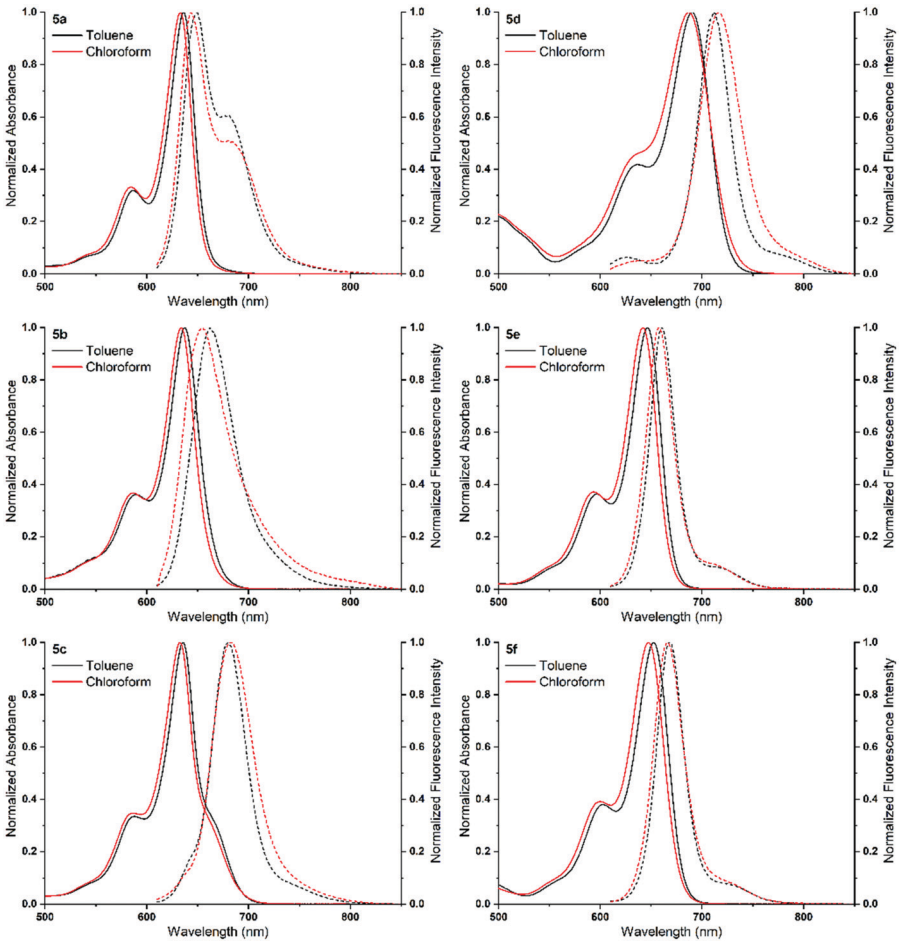


Fig. 2 Normalized absorption spectra (solid lines) for BODIPYs **5a–f** and their corresponding normalized fluorescence emission spectra (dashed lines; $\lambda_{exc}$ = 605 nm) in toluene and chloroform.

Dyad **5d**, carrying the diphenylamine donor, afforded the largest bathochromic shift (190 nm) with respect to the initial BODIPY core **2**, with an absorption maximum around 690 nm. The relative positions of the absorption maxima of the different materials nicely reflect the trends in the calculated $S_1$ energies (Table 1). The absorption profiles resemble these of typical BODIPY dyes as they are sharp and have a high-energy absorption shoulder. The phenothiazine and diphenylamine-functionalized dyads have slightly different spectra. BODIPY **5c** shows a second, red-shifted shoulder, while the absorption band of BODIPY **5d** is clearly broadened. In the UV region, an absorption peak around 350 nm is observed in all cases, originating from the distyryl extension of the BODIPY core (Fig. S9 and Table S3, ESI†). Other UV peaks are related to the incorporated donor. Absorption profiles in toluene solution almost entirely coincide with those in chloroform, although being slightly red-shifted (~4 nm).

As it is known that phenothiazine units can afford dual stable conformers, a relaxed potential energy surface scan was performed for compound **5c** using the M06-2X/6-311G(d) method (Fig. S10, ESI†).[74] This revealed the existence of a

 

Table 3 Spectroscopic data for BODIPY dyads **5a–f** as obtained in toluene and chloroform solution[a]

| BODIPY | Solv.[b] | $\lambda_{abs}$[c] (nm) | $\lambda_{em}$[d] (nm) | $\Delta\bar{\nu}$[e] ($cm^{-1}$) | $fwhm_{abs}$[f] ($cm^{-1}$) | $fwhm_{em}$[g] ($cm^{-1}$) | $\varepsilon$[h] ($M^{-1}cm^{-1}$) | $\Phi_f$[i] | $\Phi_\Delta$[j] | BT[k] ($M^{-1}$ $cm^{-1}$) | PP ($M^{-1}$ $cm^{-1}$)[l] |
|---|---|---|---|---|---|---|---|---|---|---|---|
| **5a** | TOL | 636 | 649 | 323 | 744 | 1333 | $1.24 \times 10^5$ | 0.69 ± 0.03 | 0.07 ± 0.01 | 86 200 | 9000 |
| | CL | 633 | 645 | 294 | 777 | 917 | $1.20 \times 10^5$ | 0.63 ± 0.03 | 0.23 ± 0.02 | 75 200 | 27 000 |
| **5b** | TOL | 638 | 663 | 592 | 884 | 1086 | $1.05 \times 10^5$ | 0.47 ± 0.00 | 0.47 ± 0.03 | 49 200 | 49 900 |
| | CL | 634 | 653 | 459 | 882 | 1165 | $9.48 \times 10^4$ | <0.01 | 0.37 ± 0.02 | 400 | 35 100 |
| **5c** | TOL | 636 | 680 | 1017 | 867 | 777 | $1.12 \times 10^5$ | 0.53 ± 0.00 | 0.33 ± 0.01 | 59 600 | 36 900 |
| | CL | 633 | 683 | 1156 | 913 | 987 | $1.00 \times 10^5$ | 0.05 ± 0.00 | 0.38 ± 0.01 | 5500 | 37 900 |
| **5d** | TOL | 691 | 712 | 427 | 1033 | 729 | $1.06 \times 10^5$ | 0.47 ± 0.01 | 0.06 ± 0.01 | 49 700 | 6300 |
| | CL | 687 | 716 | 589 | 1304 | 916 | $9.63 \times 10^4$ | 0.43 ± 0.00 | 0.06 ± 0.00 | 40 900 | 5600 |
| **5e** | TOL | 647 | 661 | 339 | 858 | 659 | $1.16 \times 10^5$ | 0.73 ± 0.02 | 0.04 ± 0.03 | 83 900 | 5100 |
| | CL | 642 | 658 | 379 | 883 | 721 | $1.19 \times 10^5$ | 0.75 ± 0.01 | 0.06 ± 0.01 | 88 800 | 7300 |
| **5f** | TOL | 653 | 669 | 367 | 915 | 696 | $1.18 \times 10^5$ | 0.71 ± 0.01 | 0.01 ± 0.01 | 83 ,100 | 1300 |
| | CL | 648 | 667 | 440 | 988 | 773 | $1.06 \times 10^5$ | 0.70 ± 0.01 | 0.02 ± 0.01 | 74 200 | 2000 |

[a] All values are averaged over three independent measurements. [b] Spectrograde solvents were used for all measurements; TOL = toluene, CL = chloroform. [c] Absorption maximum. [d] Fluorescence emission maximum. [e] Energy difference between the absorption and emission maxima. [f] Full-width-at-half-maximum of the absorption band. [g] Full-width-at-half-maximum of the emission band. [h] Molar attenuation coefficient. [i] Fluorescence quantum yield determined *vs.* nile blue ($\Phi_f$ = 0.27, $\lambda_{exc}$ = 605 nm in spectrograde ethanol). Standard deviations are reported. [j] Singlet oxygen quantum yield determined *vs.* methylene blue ($\Phi_\Delta$ = 0.52, $\lambda_{exc}$ = 639 nm in spectrograde ethanol) by monitoring the absorbance of 1,3-DPBF at 414 nm. Standard deviations are reported. [k] Fluorescence brightness. [l] Phototoxic power.

slightly more stable conformer wherein one phenothiazine donor unit has a much smaller dihedral angle with the distyryl substituent, albeit being bent out of plane (Fig. S11, ESI†). This conformer is henceforth termed the 'coplanar' conformer for convenience. (TD)DFT calculations were repeated for this conformer and are presented in Tables S4, S5 and Fig. S12 (ESI†). We observed a slightly lower $S_1$ state compared to the perpendicular conformer (Table 1), providing a possible explanation for the presence of the red absorption shoulder for **5c** in Fig. 2. Despite the larger calculated oscillator strength for the coplanar conformer, this red-shifted absorption is, however, of lower intensity. In addition, the coplanar conformer is not observed in the single-crystal structure and therefore it is considered to be less present and of little importance for the further discussion.

For the six BODIPY dyes, the emission maxima are close to their absorption counterparts, resulting in small Stokes shifts, both in chloroform and toluene solution. For phenothiazine-BODIPY dyad **5c**, the difference between the absorption and emission maxima reaches over 1000 $cm^{-1}$. This large offset is of interest for future PDT applications, since it limits interference between the activation light and the emitted fluorescence. For BODIPYs **5b, c**, only one (strongly tailing) fluorescence peak is seen. For the other donors **5a, d–f**, a low-energy emission shoulder of varying relative intensity is noticed. For a better visualization of the spectroscopic differences within the complete series, the absorption and emission profiles were plotted together in a separate figure for each solvent in Fig. S13 (ESI†).

$\Phi_f$ and $\Phi_\Delta$ values depend on the type of donor introduced and differ significantly. Generally, the fluorescence ability decreases compared to BODIPY precursor **2** ($\Phi_f$ = 0.97 in dichloromethane),[75] as expected for red-shifted dyes due to the energy-gap law. However, these values are still significant, retaining a $\Phi_f$ of at least 40% in chloroform as well as in toluene solution for dyads **5a, d–f**. The brightest variants are obtained with dimethylacridine (**5a**), carbazole (**5e**), and di-*tert*-butylcarbazole (**5f**) donors, with quantum yields around 70%. BODIPYs **5b, c** are somewhat peculiar as their emission is almost negligible in chloroform, but close to 50% in toluene. According to $\Phi_\Delta$, we can divide the six dyads into two groups, in line with our observations on the D–A dihedral angles given in Fig. 1. The BODIPY materials based on diphenylamine and both carbazole donors (**5d–f**; $\theta_{D-A} < 90^\circ$) are unable to produce a considerable amount of $^1O_2$ during excitation at 639 nm (around or below 6%). On the other hand, dimethylacridine, phenoxazine, and phenothiazine (**5a–c**; $\theta_{D-A} = 90^\circ$) afford suitable PSs with $^1O_2$ quantum yields of 23, 37, and 38% in chloroform, respectively. The $\Phi_\Delta$ value for the dimethylacridine-based dyad **5a** in toluene drops below 10%. Interestingly, this is not the case for phenoxazine and phenothiazine dyads **5b–c**, where $^1O_2$ production is still significant, with yields of 47 and 33%, respectively. Hence, the combination of strong fluorescence and $^1O_2$ formation, together with their high molar attenuation coefficients, renders these new distyryl-BODIPY dyes promising dual-functioning PSs.

### Solvent- and concentration-dependent fluorescence

At this stage, the underlying mechanism explaining the differences in $\Phi_\Delta$ remains unclear. TDDFT calculations (Table 2) showed that ISC *via* intermediate CT states (SOCT-ISC), as often proposed in literature for push–pull type (BODIPY) dyes, seems unlikely as there is no available CT state.[40–42,47,48] The presence of CT states can be revealed photophysically by evaluating the fluorescence profiles in solvents of different polarity. As CT states are highly polar excited states, a polar medium stabilizes them. Hence, CT bands typically display a bathochromic shift in polar solvents. Furthermore, CT bands initially absent in an apolar solvent can be revealed in polar medium as the CT state might become more populated and/or emissive relaxation toward the ground state is favored as a result of the changed CT energy. Additional measurements were hence performed in the more polar solvents acetone, dimethyl sulfoxide (DMSO), and acetonitrile (Fig. S9, S13–S14 and Tables S3, S6, ESI†).

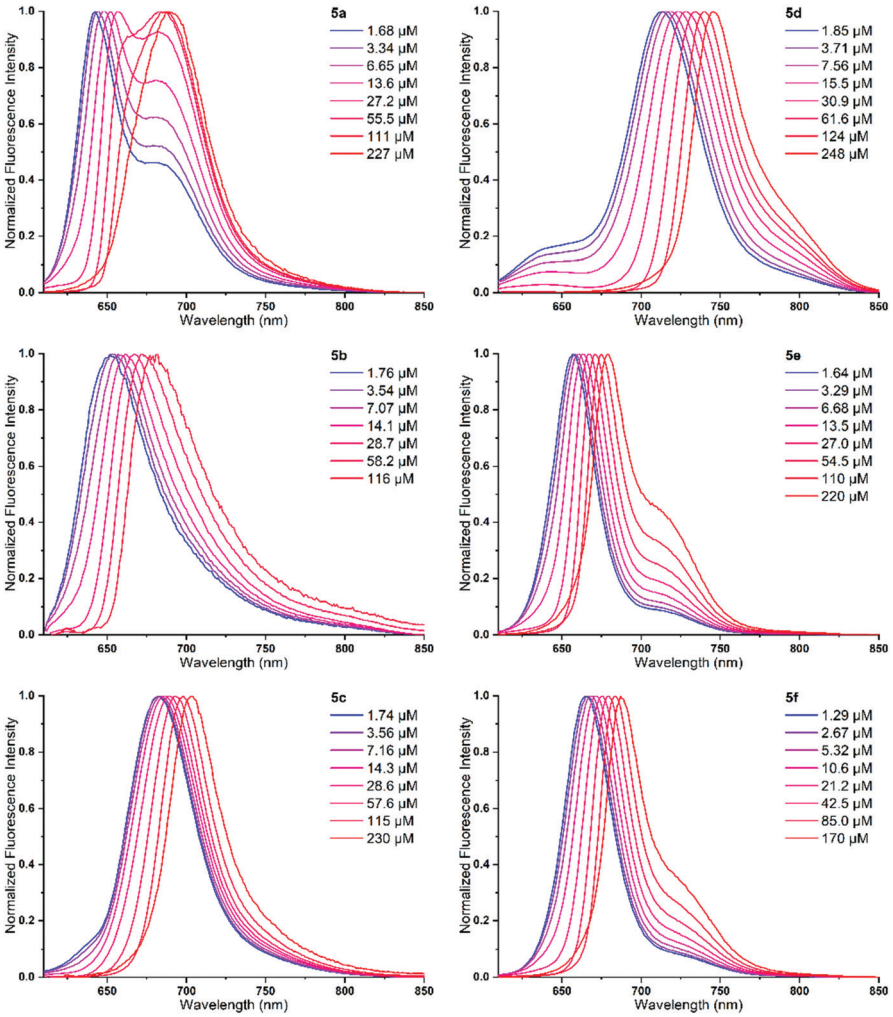


Fig. 3 Normalized fluorescence emission spectra for a dilution series of BODIPYs **5a–f** in chloroform ($\lambda_{exc}$ = 605 nm).

For dyads **5d–f**, no meaningful influence of solvent polarity on the emission profile was observed. The fluorescence of BODIPYs **5a–c** did vary to some extent between polar and apolar solvents. For the dyads with phenoxazine (**5b**) and phenothiazine (**5c**), a potential CT band can be distinguished. However, the nearly completely quenched fluorescence in **5a–c** (Table S6, ESI†) renders these observations rather inconclusive.

In our previous work on BODIPY-dimethylacridine dyads (**5a**), we suggested that ISC could possibly proceed *via* an exciplex intermediate state ($^1$EX).[66] Hence, a similar screening of the fluorescence profile at different concentrations was performed for BODIPYs **5b–f** (Fig. 3 and Fig. S15–S17, ESI†).

A bathochromic shift in the fluorescence maxima was observed for the six BODIPYs upon increasing concentration. This is a commonly observed phenomenon, whereby the increased molecular interaction enlarges the perceived Stokes shift (inner filter effect).[76] As previously described, dyad **5a** shows a strong increase in relative intensity of a second emission band as the concentration increases.[66] In diluted samples, the localized singlet state ($^1$LE) emission at 645 nm is most intense. As concentration increases, the relative population of the $^1$LE and $^1$EX band is altered, and the exciplex state becomes more distinct. This trend results in an exciplex band ($\lambda_{em,EX}$ = 690 nm) that transcends the $^1$LE emission. At high concentration, the $^1$LE emission even disappeared completely, with only the emission from the $^1$EX state remaining. Similar behavior is observed in toluene (Fig. S14, ESI†). For the other dyads (**5b–f**), this remarkable behavior is not explicitly visible (Fig. 3 and Fig. S15, ESI†). A slight increase of the long-wavelength fluorescence shoulder can be noticed for BODIPYs **5d–f** upon increasing concentration, but not at all to the same extent as for **5a**. Furthermore, the dyads with phenoxazine and phenothiazine donors (**5b–c**) do not show a second emission band resulting from molecular aggregation, despite their ISC ability. Hence, exciplex formation seems to occur only for dyad **5a**, whereas BODIPYs **5b–c** have to rely on another mechanism to explain their high $^1O_2$ generation capabilities upon photo-excitation. To get a better idea of the relative fluorescence intensities at different concentrations, these data were also normalized to the concentration (Fig. S16 and S17, ESI†). In all cases, a strong quenching of the emissive behavior was observed upon increasing concentration.

 

### Femtosecond transient absorption spectroscopy

Transient absorption spectra, achieved with a high time resolution of ~30 fs, were recorded to gain additional information on the ultrafast excited state evolutions of the dyads. All samples were excited using a broadband ultrashort pulse (<30 fs) covering the 550–760 nm spectral range. A second broadband ultrashort pulse was used as the probe beam. Transient spectra were acquired within a pump–probe time delay window of 200 ps. The raw transient absorption spectra are shown in Fig. S18 and S19 (ESI†). To extract the time constants associated with the excited state evolution, a global fitting of the kinetic traces was performed using a sequential linear kinetic scheme (using the software Glotaran).[77] The evolution-associated difference spectra (EADS) obtained from global analysis for BODIPYs **5a–f** in toluene solution are reported in Fig. 4. Global analysis was also performed on the transient data of dyads **5a–f** in chloroform solution (Fig. S20, ESI†). The EADS are very similar to those obtained in toluene solution, although there are small differences in the extracted kinetic constants. To facilitate the analysis of the new dyads, a reference compound lacking a donor moiety (distyryl-BODIPY **5H**, donor = H in Scheme 1) was synthesized and transient spectra were acquired for this compound as well (see Fig. S21 and the associated discussion in the ESI†).

Considering the newly synthesized dyads **5a–f**, whose EADS are reported in Fig. 4, the most intense signal is a negative band whose position matches well with the absorption maximum (Fig. 2) and can thus be assigned to ground-state bleaching (GSB). Besides, differences are observed for the smaller intensity excited-state absorption (ESA) and stimulated emission (SE) bands. As noticed in Fig. 4, the EADS of BODIPYs **5b, c** are qualitatively similar. In both cases, a positive band is observed to rise on a 10–20 ps timescale in the 680–750 nm region, while the low intensity SE band is not observed for these systems. In case of phenoxazine-BODIPY **5b**, the positive signal starts rising at the short timescale since it is already observed in the second spectral component, with a rise time of 200 fs. The positive band is initially peaked at 700 nm. Within the following 5.5 ps, the ESA intensity increases and a second maximum at 730 nm

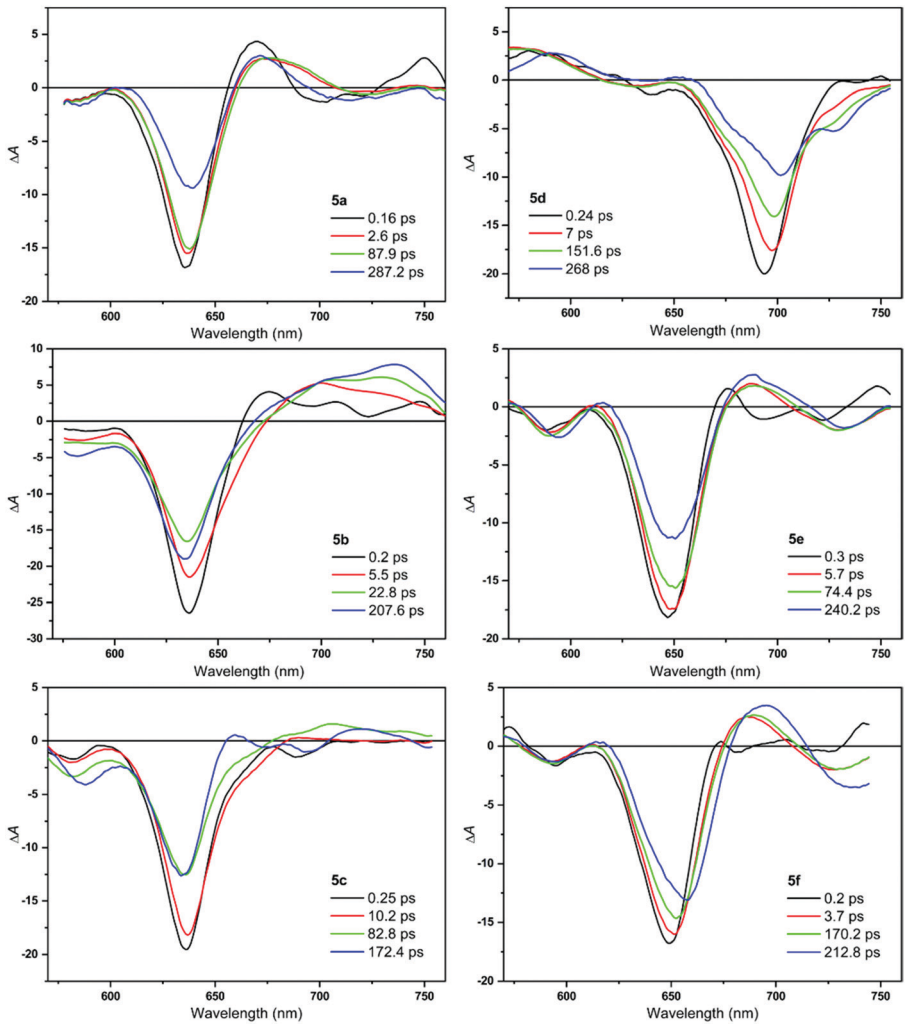


Fig. 4 Evolution-associated difference spectra (EADS) for BODIPYs **5a–f** in toluene solution as obtained by singular value decomposition (SVD) and global fitting of the transient data (target analysis).

appears. The band further rises in the evolution toward the following EADS, occurring in 23 ps. The intensity of the bleaching signal progressively recovers, and its peak slightly blue-shifts in time. For phenothiazine-BODIPY **5c**, the rise of the positive band appears slower as compared to **5b**. Indeed, a positive band peaked at 700 nm is clearly observed only in the third spectral component, rising in 10 ps. In the following EADS, a negative signal appears in the 660–700 nm region, while two positive peaks are visible at 650 and 710 nm. The appearance of a positive band on the red side of the bleaching band can point to the occurrence of charge separation between the BODIPY core and the donor substituents. Indeed, it was previously indicated that the localization of a negative charge on the BODIPY core induces the appearance of an absorption band on the red side of the GSB of the correspondent neutral species.[64,78–80] The spectral evolution observed for dyad **5c** on the 83 ps timescale could point to a structural relaxation of the charge-separated state (CSS).

The occurrence of charge separation is less clear in case of BODIPY **5a**. The transient spectra registered in the two solvents are very similar (Fig. 4 and Fig. S20, ESI†). The initial EADS resembles that of the distyryl BODIPY without a donor moiety (**5H**; Fig. S21, ESI†). The signal evolves in 160 fs, with the ESA band broadening and compensating the SE band. The spectral shape remains almost unvaried in the following evolution (2.6 ps), while in the subsequent evolution (88 ps) both the GSB and ESA band decrease in intensity. A small SE signal is again visible in the final spectral component because of the decreased intensity of the positive signal in the same region. The rise of a positive signal in the 700 nm region could indicate the presence of a CSS. However, the kinetics of this process are different compared to what was observed for BODIPYs **5b, c**. Comparing the kinetic traces recorded on the ESA band of compounds **5a–c** (Fig. S22, ESI†), it can be noticed that the positive band in **5b, c** rises on a similar timescale of a few tens of ps, while the rise for **5a** is much faster and is followed by a faster decay. Comparison of the transient absorption data thus suggests that the ISC mechanism for these dyes might be different, with triplet formation possibly mediated by the presence of exciplexes in case of dimethylacridine-BODIPY **5a** and charge separation/recombination for phenoxazine- and phenothiazine-BODIPYs **5b, c**.

The EADS of BODIPYs **5d–f** are qualitatively different from those of BODIPYs **5a-c** (Fig. 4 and Fig. S20, ESI†). In particular, the EADS of carbazole-BODIPYs **5e, f** closely resemble those of the distyryl-BODIPY **5H**, although red-shifted. The ESAs observed in these compounds, peaked at 688 and 700 nm, respectively, have a very fast rise, suggesting that this signal is associated to the bright $S_1$ state. This is clearly shown by the comparison of the kinetic traces recorded on the ESAs of **5b** and **5f** shown in Fig. S23 (ESI†). The spectra of diphenylamine–BODIPY **5d** are different, reflecting the strong red-shift in the absorption observed for this sample. Indeed, in this case, the bleaching signal is located at 693 nm and an ESA band is observed in the blue part of the investigated spectral region (560 nm). Following the time evolution, the bleaching progressively recovers, while a SE band appears around 730 nm. This band progressively increases in intensity and slightly red-shifts, signaling the occurrence of emission by a relaxed excited state. Nevertheless, also in this case there is no indication of the involvement of other excited states in the dynamics, which thus proceeds through relaxation from the bright $S_1$ state.

To gain additional information on the occurrence of charge separation and the differences observed in dyads **5a–c** as compared to **5d–f**, transient spectra of two representative compounds for each group, namely **5b** and **5e**, were measured on an extended timescale reaching 1.5 ns pump–probe delay. The EADS obtained by performing a global analysis on these data, in both chloroform and toluene, are reported in the supplementary information (Fig. S24 and S25 (ESI†) and related comments). By inspection of the EADS, it can be noticed that the excited state dynamics on the timescale $>200$ ps are highly influenced by solvent polarity in case of BODIPY **5b**, as is expected in case of charge separation. Indeed, the transient spectra recover almost completely within the 1.5 ns timescale in chloroform, suggesting the occurrence of charge recombination, while slower dynamics are observed in toluene. In case of **5e**, both the spectral shape and the spectral evolution are almost independent on solvent polarity.

### Excited state geometry optimizations

Since the femtosecond transient absorption spectra suggest the presence of an intermediate state with CT character in BODIPY dyads **5b, c** (Fig. 4), whereas there is no evidence of the involvement of this state from TDDFT calculations on the ground state geometry (Table 2), excited state geometry optimizations were performed to probe the effects of geometrical relaxation. While higher level methods such as riCC2 or CASPT2 are preferred to optimize the excited state geometries of molecules exhibiting CT character, it has been shown that XC functionals with significant amounts of Hartree–Fock exchange, such as M06-2X or long-range corrected XC functionals such as CAM-B3LYP, give reasonable results with respect to these higher level methods or experimental results.[81–83] Since higher level methods (riCC2, CASPT2, *etc.*) are too computationally demanding for these molecules, the same level of approximation as applied for the ground state optimizations (M062X/6-311G(d)) was used. The excited state geometries for the first (LE character) and second (CT character) excited states were optimized in the gas phase. Upon relaxation, the first singlet excited states of BODIPYs **5a, b** show smaller D–A dihedral angles of 82° and 64°, respectively (Fig. S26 and S27, ESI†). For BODIPY **5c**, this is not the case (Fig. S28, ESI†). BODIPYs **5d–f** do not show significant differences in the D–A dihedral angles as compared to the ground states either (Fig. S29–S31, ESI†). The decrease in dihedral angle for **5a, b** leads to a delocalization of the HOMO onto the donor and distyryl–BODIPY fragments and mixes CT and LE character for the first singlet excited state (Fig. S26,S27 and Table S7, ESI†). For **5b**, this effect is much stronger due to the strongly reduced dihedral angle with respect to the ground state geometry. When optimizing the second singlet excited state, the D–A dihedral angles remain unchanged as compared to the

 

ground state (Fig. S26–S31, ESI†). The $S_1$–$S_2$ energy difference ($\Delta E_{S1-S2}$) remains unchanged for BODIPYs **5d–f** and no mixing of CT and LE character is observed for these molecules. However, a strong decrease of $\Delta E_{S1-S2}$ is observed for BODIPYs **5a** and (in particular) **5b**, indicating that the excited states are close in energy for this given geometry (Table S8, ESI†). For dyad **5c**, we were unable to optimize the second singlet excited state due to a rearrangement of the energy levels during the optimization procedure. We do observe that the vertical de-excitation energies of $S_1$ and $S_2$ come very close and even invert before the energy level rearrangement occurs. These results indicate that after excited state relaxation, the LE and CT excited states come closer in energy for BODIPYs **5b, c** thus enabling a mixing between them. This is in line with the findings of the femtosecond transient absorption experiments and further solidifies the hypothesis that a CT state is involved in the ISC process.

Involvement of CT states also allows to clarify the strong solvent dependence of the fluorescence intensity of **5b, c** (Table 3). As CT states are highly polar excited states, their energy is strongly affected by the surrounding medium.[84] In a more polar solvent (*e.g.* chloroform), the CT state is stabilized, thereby decreasing its energy. However, the approach of the CT state to the ground state induces more radiationless relaxation. Accordingly, dyads **5b, c** show quenched emission in chloroform. In relatively apolar toluene solution, a larger singlet state population is retained, preserving the fluorescence.

## Conclusions

A series of six different distyryl–BODIPY–donor dyads were synthesized and the photophysical properties were evaluated with an eye on their potential application as photosensitizers in image-guided photodynamic therapy. All dyes show strong absorption in the phototherapeutic window. The main differences are found in their brightness and phototoxic behavior. BODIPYs bearing diphenylamine or carbazole donors show moderate to strong fluorescence, respectively, but produce very little singlet oxygen upon photoexcitation. Dimethylacridine, phenoxazine, and phenothiazine donors are oriented perpendicularly with respect to the styryl moieties in the ground state geometry. This seems to be an essential structural feature as, next to a moderate fluorescence quantum yield, these dyads afford significant singlet oxygen quantum yields without the aid of heavy atoms. Phenoxazine- and phenothiazine-bearing BODIPYs show improved photosensitizer characteristics with respect to the earlier reported dimethylacridine–distyryl BODIPY dyads. With $\Phi_f$ = 53% and $\Phi_\Delta$ = 33% for phenothiazine, and $\Phi_f = \Phi_\Delta$ = 47% for phenoxazine (in toluene), these new dyads can be considered as highly promising dual-functioning photosensitizers. The intersystem crossing mechanism in the BODIPY dyads was studied using femtosecond transient absorption spectroscopy. Charge separation/recombination seems to take place in the phenoxazine- and phenothiazine-based molecules. This hypothesis was further solidified by optimizing the first and second excited state geometries, revealing their relatively small energy difference, allowing mixing between them. Further improvements with respect to the donor could be explored toward even more efficient BODIPY photosensitizers. However, one should be aware that several other factors come into play besides merely donor strength. Although a new donor could improve charge-transfer characteristics, other variables (*e.g.* geometry, redox potential, dipole moment, charge recombination) will change as well, thereby affecting the overall phototoxicity. Balancing these effects remains the key toward high-performance dual photosensitizers. In any case, due to the promising results for our present donor–acceptor BODIPY dyads, further steps will already be taken to probe their behavior in biological media with an eye on future *in vitro* and *in vivo* examinations.

## Conflicts of interest

There are no conflicts of interest to declare.

## Acknowledgements

The authors thank Hasselt University and the University of Namur for continuing financial support (PhD scholarships JD and TC). BC and WM thank the Research Foundation – Flanders (FWO) for support through projects G087718N, G0D1521N, I006320N, GOH3816NAUHL, and the Scientific Research Community 'Supramolecular Chemistry and Materials' (W000620N). The calculations were performed on the computers of the 'Consortium des équipements de Calcul Intensif (CÉCI)' (**https://www.ceci-hpc.be**), including those of the 'UNamur Technological Platform of High-Performance Computing (PTCI)' (**https://www.ptci.unamur.be**), for which we gratefully acknowledge financial support from the FNRS-FRFC, the Walloon Region, and the University of Namur (Conventions no. 2.5020.11, GEQ U.G006.15, U.G018.19, 1610468, and RW/GEQ2016). SD, AL, and MDD acknowledge support from the European Union's Horizon 2020 research and innovation program under grant agreement no. 871124 Laserlab-Europe.

## References

1 M. C. DeRosa and R. J. Crutchley, *Coord. Chem. Rev.*, 2002, **233**, 351–371.
2 J. Moan, *J. Photochem. Photobiol., B*, 1990, **6**, 343–347.
3 J. Moan and K. Berg, *Photochem. Photobiol.*, 1991, **53**, 549–553.
4 S. Kwiatkowski, B. Knap, D. Przystupski, J. Saczko, E. Kedzierska, K. Knap-Czop, J. Kotlinska, O. Michel, K. Kotowski and J. Kulbacka, *Biomed. Pharmacother.*, 2018, **106**, 1098–1107.
5 H. I. Pass, *J. Natl. Cancer Inst.*, 1993, **85**, 443–456.
6 W. M. Sharman, C. M. Allen and J. E. van Lier, *Drug Discovery Today*, 1999, **4**, 507–517.
7 T. J. Dougherty, *J. Clin. Laser Med. Sur.*, 2002, **20**, 3–7.
8 M. R. Hamblin and T. Hasan, *Photochem. Photobiol. Sci.*, 2004, **3**, 436–450.
9 Z. Huang, *Technol. Cancer Res. Treat.*, 2005, **4**, 283–293.

10 M. A. MacCormack, *Semin. Cutaneous Med. Surg.*, 2008, **27**, 52–62.
11 P. Babilas, S. Schreml, M. Landthaler and R. M. Szeimies, *Photodermatol., Photoimmunol. Photomed.*, 2010, **26**, 118–132.
12 T. Dai, B. B. Fuchs, J. J. Coleman, R. A. Prates, C. Astrakas, T. G. Denis, M. S. Ribeiro, E. Mylonakis, M. R. Hamblin and G. P. Tegos, *Front. Microbiol.*, 2012, **3**, 120–136.
13 C. S. Foote, *Photochem. Photobiol.*, 1991, **54**, 659.
14 A. P. Castano, T. N. Demidova and M. R. Hamblin, *Photodiagn. Photodyn. Ther.*, 2004, **1**, 279–293.
15 V. Kral, J. Davis, A. Andrievsky, J. Kralova, A. Synytsya, P. Pouckova and J. L. Sessler, *J. Med. Chem.*, 2002, **45**, 1073–1078.
16 S. J. Wagner, *Transfus. Med. Rev.*, 2002, **16**, 61–66.
17 R. R. Allison, G. H. Downie, R. Cuenca, X. H. Hu, C. J. Childs and C. H. Sibata, *Photodiagn. Photodyn. Ther.*, 2004, **1**, 27–42.
18 M. R. Detty, S. L. Gibson and S. J. Wagner, *J. Med. Chem.*, 2004, **47**, 3897–3915.
19 A. E. O'Connor, W. M. Gallagher and A. T. Byrne, *Photochem. Photobiol.*, 2009, **85**, 1053–1074.
20 S. Swavey and M. Tran, in *Recent Advances in the Biology, Therapy and Management of Melanoma*, ed. L. Davids, IntechOpen, London, 2013, ch. 11, pp. 254–282.
21 R. D. Teo, J. Y. Hwang, J. Termini, Z. Gross and H. B. Gray, *Chem. Rev.*, 2017, **117**, 2711–2729.
22 S. D'Alessandro and R. Priefer, *J. Drug Delivery Sci. Technol.*, 2020, **60**, 101979.
23 J. Deckers, T. Cardeynaels, L. Lutsen, B. Champagne and W. Maes, *Chem. Phys. Chem.*, 2021, **22**, 1488–1496.
24 S. G. Awuah and Y. You, *RSC Adv.*, 2012, **2**, 11169–11183.
25 L. Yao, S. Z. Xiao and F. J. Dan, *J. Chem.*, 2013, 1–10.
26 A. Kamkaew, S. H. Lim, H. B. Lee, L. V. Kiew, L. Y. Chung and K. Burgess, *Chem. Soc. Rev.*, 2013, **42**, 77–88.
27 C. S. Kue, S. Y. Ng, S. H. Voon, A. Kamkaew, L. Y. Chung, L. V. Kiew and H. B. Lee, *Photochem. Photobiol. Sci.*, 2018, **17**, 1691–1708.
28 L. Huang and G. Han, *Small Methods*, 2018, **2**, 1700370.
29 A. Turksoy, D. Yildiz and E. U. Akkaya, *Coord. Chem. Rev.*, 2019, **379**, 47–64.
30 W. Sun, X. Zhao, J. Fan, J. Du and X. Peng, *Small*, 2019, **15**, 1804927.
31 M. L. Agazzi, M. B. Ballatore, A. M. Durantini, E. N. Durantini and A. C. Tomé, *J. Photochem. Photobiol., C*, 2019, **40**, 21–48.
32 D. Chen, Z. Zhong, Q. Ma, J. Shao, W. Huang and X. Dong, *ACS Appl. Mater. Interfaces*, 2020, **12**, 26914–26925.
33 P. Chinna Ayya Swamy, G. Sivaraman, R. N. Priyanka, S. O. Raja, K. Ponnuvel, J. Shanmugpriya and A. Gulyani, *Coord. Chem. Rev.*, 2020, **411**, 213233.
34 W. Lin, D. Colombani-Garay, L. Huang, C. Duan and G. Han, *WIREs Nanomed. Nanobiotechnol.*, 2020, **12**, 1627.
35 R. Prieto-Montero, A. Prieto-Castañeda, R. Sola-Llano, A. R. Agarrabeitia, D. Garcia-Fresnadillo, I. López-Arbeloa, A. Villanueva, M. J. Ortiz, S. de la Moya and V. Martínez-Martínez, *Photochem. Photobiol.*, 2020, **96**, 458–477.
36 W. Zhang, A. Ahmed, H. Cong, S. Wang, Y. Shen and B. Yu, *Dyes Pigm.*, 2021, **185**, 108937.
37 A. Loudet and K. Burgess, *Chem. Rev.*, 2007, **107**, 4891–4932.
38 G. Ulrich, R. Ziessel and A. Harriman, *Angew. Chem., Int. Ed.*, 2008, **47**, 1184–1201.
39 N. Boens, B. Verbelen and W. Dehaen, *Eur. J. Org. Chem.*, 2015, 6577–6595.
40 J. Zhao, K. Xu, W. Yang, Z. Wang and F. Zhong, *Chem. Soc. Rev.*, 2015, **44**, 8904–8939.
41 K. Chen, Y. Dong, X. Zhao, M. Imran, G. Tang, J. Zhao and Q. Liu, *Front. Chem.*, 2019, **7**, 1–14.
42 J. Wang, Q. B. Gong, L. Wang, E. H. Hao and L. J. Jiao, *J. Porphyrins Phthalocyanines*, 2020, **24**, 603–635.
43 G. Kubheka, B. Babu, E. Prinsloo, N. Kobayashi, J. Mack and T. Nyokong, *J. Porphyrins Phthalocyanines*, 2020, **25**, 47–55.
44 J. Zhao, W. Wu, J. Sun and S. Guo, *Chem. Soc. Rev.*, 2013, **42**, 5323–5351.
45 J. Zhao, K. Chen, Y. Hou, Y. Che, L. Liu and D. Jia, *Org. Biomol. Chem.*, 2018, **16**, 3692–3701.
46 Y. Hou, X. Zhang, K. Chen, D. Liu, Z. Wang, Q. Liu, J. Zhao and A. Barbon, *J. Mater. Chem. C*, 2019, **7**, 12048–12074.
47 M. A. Filatov, *Org. Biomol. Chem.*, 2020, **18**, 10–27.
48 V. N. Nguyen, Y. Yan, J. Zhao and J. Yoon, *Acc. Chem. Res.*, 2021, **54**, 207–220.
49 J. P. Celli, B. Q. Spring, I. Rizvi, C. L. Evans, K. S. Samkoe, S. Verma, B. W. Pogue and T. Hasan, *Chem. Rev.*, 2010, **110**, 2795–2838.
50 S. S. Kelkar and T. M. Reineke, *Bioconjugate Chem.*, 2011, **22**, 1879–1903.
51 X. Chen and S. T. C. Wong, *Cancer Theranostics*, Academic Press, Oxford, 2014.
52 T. J. Dougherty and S. L. Marcus, *Eur. J. Cancer*, 1992, **28**, 1734–1742.
53 K. Plaetzer, B. Krammer, J. Berlanda, F. Berr and T. Kiesslich, *Lasers Med. Sci.*, 2009, **24**, 259–268.
54 K. Deng, C. Li, S. Huang, B. Xing, D. Jin, Q. Zeng, Z. Hou and J. Lin, *Small*, 2017, **13**, 1702299.
55 A. B. Descalzo, H. J. Xu, Z. Shen and K. Rurack, *Ann. N. Y. Acad. Sci.*, 2008, **1130**, 164–171.
56 L. Yuan, W. Lin, K. Zheng, L. He and W. Huang, *Chem. Soc. Rev.*, 2013, **42**, 622–661.
57 Y. Ni and J. Wu, *Org. Biomol. Chem.*, 2014, **12**, 3774–3791.
58 H. Lu, J. Mack, Y. Yang and Z. Shen, *Chem. Soc. Rev.*, 2014, **43**, 4778–4823.
59 S. G. Awuah, S. K. Das, F. D'Souza and Y. You, *Chem. – Asian J.*, 2013, **8**, 3123–3132.
60 R. L. Watley, S. G. Awuah, M. Bio, R. Cantu, H. B. Gobeze, V. N. Nesterov, S. K. Das, F. D'Souza and Y. You, *Chem. – Asian J.*, 2015, **10**, 1335–1343.
61 Z. Wang, L. Huang, Y. Yan, A. M. El-Zohry, A. Toffoletti, J. Zhao, A. Barbon, B. Dick, O. F. Mohammed and G. Han, *Angew. Chem., Int. Ed.*, 2020, **59**, 16114–16121.
62 H. Ito, H. Sakai, Y. Suzuki, J. Kawamata and T. Hasobe, *Chem. – Eur. J.*, 2020, **26**, 316–325.
63 Y. Hou, Q. Liu and J. Zhao, *Chem. Commun.*, 2020, **56**, 1721–1724.
64 Y. Dong, A. Elmali, J. Zhao, B. Dick and A. Karatay, *Chem. Phys. Chem.*, 2020, **21**, 1388–1401.

 

65 G. Turkoglu, G. Kayadibi Koygun, M. N. Z. Yurt, N. Demirok and S. Erbas-Cakmak, *Org. Biomol. Chem.*, 2020, **18**, 9433–9437.
66 J. Deckers, T. Cardeynaels, H. Penxten, A. Ethirajan, M. Ameloot, M. Kruk, B. Champagne and W. Maes, *Chem. – Eur. J.*, 2020, **26**, 15212–15225.
67 As the exact structure of these ''exciplexes' (*i.e.* excited state complexes) remains unknown for now, we propose to use this more general term.
68 A. C. Benniston, G. Copley, H. Lemmetyinen and N. V. Tkachenko, *Chem. Phys. Chem.*, 2010, **11**, 1685–1692.
69 A. C. Benniston, A. Harriman, V. L. Whittle, M. Zelzer, R. W. Harrington and W. Clegg, *Photochem. Photobiol. Sci.*, 2010, **9**, 1009–1017.
70 A. Nano, R. Ziessel, P. Stachelek, M. A. Alamiry and A. Harriman, *Chem. Phys. Chem.*, 2014, **15**, 177–186.
71 Y. Rong, C. Wu, J. Yu, X. Zhang, F. Ye, M. Zeigler, M. E. Gallina, I. C. Wu, Y. Zhang, Y. H. Chan, W. Sun, K. Uvdal and D. T. Chiu, *ACS Nano*, 2013, **7**, 376–384.
72 H. Y. Yang, M. Zhang, J. W. Zhao, C. P. Pu, H. Lin, S. L. Tao, C. J. Zheng and X. H. Zhang, *Chin. J. Chem.*, 2022, **40**, 911–917.
73 T. Le Bahers, C. Adamo and I. Ciofini, *J. Chem. Theory Comput.*, 2011, **7**, 2498–2506.
74 K. Wang, Y. Z. Shi, C. J. Zheng, W. Liu, K. Liang, X. Li, M. Zhang, H. Lin, S. L. Tao, C. S. Lee, X. M. Ou and X. H. Zhang, *ACS Appl. Mater. Interfaces*, 2018, **10**, 31515–31525.
75 A. B. Nepomnyashchii, M. Broring, J. Ahrens and A. J. Bard, *J. Am. Chem. Soc.*, 2011, **133**, 8633–8645.
76 J. R. Lakowicz, *Principles of Fluorescence Spectroscopy*, Springer, Boston, MA, 3 edn, 2006.
77 J. J. Snellenburg, S. P. Laptenok, R. Seger, K. M. Mullen and I. H. M. V. Stokkum, *J. Stat. Soft.*, 2012, **49**, 1–22.
78 Z. Mahmood, M. Taddei, N. Rehmat, L. Bussotti, S. Doria, Q. Guan, S. Ji, J. Zhao, M. Di Donato, Y. Huo and Y. H. Xing, *J. Phys. Chem. C*, 2020, **11**, 5944–5957.
79 Z. Wang, M. Ivanov, Y. Gao, L. Bussotti, P. Foggi, H. Zhang, N. Russo, B. Dick, J. Zhao, M. Di Donato, G. Mazzone, L. Luo and M. Fedin, *Chem. – Eur. J.*, 2020, **26**, 1091–1102.
80 M. A. Filatov, S. Karuthedath, P. M. Polestshuk, H. Savoie, K. J. Flanagan, C. Sy, E. Sitte, M. Telitchko, F. Laquai, R. W. Boyle and M. O. Senge, *J. Am. Chem. Soc.*, 2017, **139**, 6282–6285.
81 C. A. Guido, D. Jacquemin, C. Adamo and B. Mennucci, *J. Phys. Chem. A*, 2010, **114**, 13402–13410.
82 C. A. Guido, S. Knecht, J. Kongsted and B. Mennucci, *J. Chem. Theory Comput.*, 2013, **9**, 2209–2220.
83 D. Jacquemin, A. Planchat, C. Adamo and B. Mennucci, *J. Chem. Theory Comput.*, 2012, **8**, 2359–2372.
84 D. Escudero, *Acc. Chem. Res.*, 2016, **49**, 1816–1824.